ELSEVIER

A Large Acceptance Detector System (LADS)
for studies of pion absorption

LADS Collaboration

T. Alteholz[c], D. Androić[ℓ], G. Backenstoss[a], D. Bosnar[ℓ], H. Breuer[e], A. Brković[ℓ],
H. Döbbeling[k], T. Dooling[j], W. Fong[f], M. Furić[ℓ], P.A.M. Gram[d], N.K. Gregory[f],
J.P. Haas[h], A. Hoffart[c], C.H.Q. Ingram[k], A. Klein[j], K. Koch[k], J. Köhler[a], B. Kotliński[k],
M. Kroedel[a], G. Kyle[h], A. Lehmann[a], Z.N. Lin[h], G. Mahl[k], A.O. Mateos[f],
K. Michaelian[k], S. Mukhopadhyay[h], T. Petković[ℓ], M. Planinić[ℓ], R.P. Redwine[f],
D. Rowntree[f], R. Schumacher[b], U. Sennhauser[k], N. Simičević[f], F.D. Smit[g],
G. van der Steenhoven[i], D.R. Tieger[f], R. Trezeciak[c], H. Ullrich[c], M. Wang[h],
M.H. Wang[h], H.J. Weyer[a,k], M. Wildi[a], K.E. Wilson[f]

[a] University of Basel, CH-4056 Basel, Switzerland
[b] Carnegie-Mellon University, Pittsburgh, PA 15213, USA
[c] University of Karlsruhe, D-76128 Karlsruhe, Germany
[d] LAMPF, Los Alamos, NM 87545, USA
[e] University of Maryland, College Park, MD 20742, USA
[f] Massachusetts Institute of Technology, Cambridge, MA 02139, USA
[g] National Accelerator Center, Faure 7131, South Africa
[h] New Mexico State University, Las Cruces, NM 88003, USA
[i] NIKHEF-K, NL-1009 DB Amsterdam, The Netherlands
[j] Old Dominion University, Norfolk, VA 23529, USA
[k] Paul Scherrer Institute, CH-5232 Villigen PSI, Switzerland
[ℓ] University of Zagreb, HR-41001 Zagreb, Croatia

Abstract

A Large Acceptance Detector System (LADS) has been designed and built at the Paul Scherrer Institute to study multi-particle final states following pion–nucleus absorption. It consists of a 28-sector cylinder of plastic scintillators of 1.6 m active length and 1.4 m diameter, two cylindrical wire chambers, and two 14-sector plastic scintillator end-caps which close each end. The nearly 4π solid angle coverage of this detector minimizes uncertainties associated with extrapolations over unmeasured regions of phase space. The design and the performance of the LADS detector are presented.

1. Introduction

The Large Acceptance Detector System (LADS) has been designed and built at the Paul Scherrer Institute in Villigen, Switzerland. The primary goal of the detector is to probe the characteristics of pion absorption at energies around the $\Delta(1232)$-resonance, especially for reactions leading to multi-nucleon final states. Many experiments on pion absorption have seen a clear signal of quasi-free absorption on a two-nucleon pair, as expected. What was generally unexpected was the very substantial cross section which appears to involve more than two nucleons.

Corrections for initial and final state interactions of the pion and nucleons appear too weak to account for all of this multi-nucleon absorption. In the early investigations of multi-nucleon final states, combinations of small solid angle coverage, incomplete kinematic definition, and uncertain particle identification, combined in some cases with poor statistical accuracy, led to ambiguities of interpretation. LADS was built mainly to establish whether a strong multi-nucleon absorption process exists and, if so, to study its nature. For interested readers, the experimental status of pion absorption measurements may be found in recent reviews [1,2].
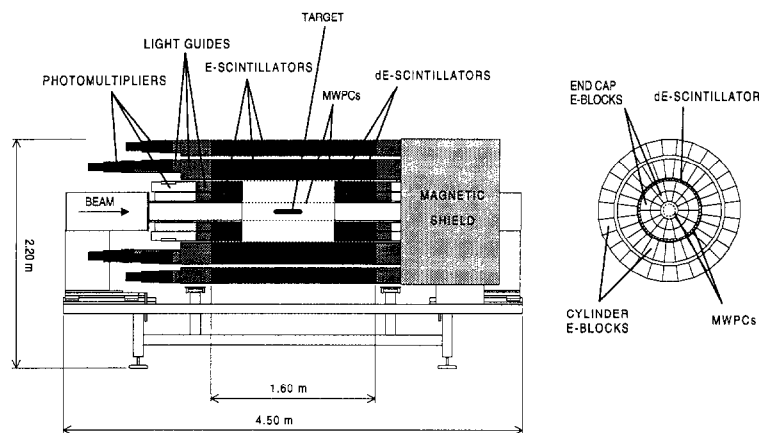
Fig. 1. A schematic view of the LADS detector.

Table 1
Some important characteristics of LADS

Geometrical acceptance	98.8% of 4π sr
Energy threshold for protons	$\approx$20 MeV
Maximum measurable proton energy	200 MeV
Energy resolution for charged particles	3–5% [FWHM]
Vertex resolution from two tracks	1 mm
Angular resolution for charged particles	$\approx$1°
Detection efficiency for neutrons	$\approx$35%
Angular resolution for neutrons	$\approx$13°

The LADS detector is a 28 sector cylinder of plastic scintillator, illustrated in Fig. 1. Two 14 sector "end-caps" of plastic scintillator close each end, and two cylindrical wire chambers define the trajectories of charged particles emerging from a target suspended near the center of the detector. Table 1 lists the primary characteristics of the detector. All of the major components of LADS are discussed below, followed by a brief discussion of some of the aspects of the analysis most closely related to the detector and by a summary of the overall performance.

2. Apparatus

2.1. Cylinder scintillators

The main cylinder of the LADS detector consists of three concentric rings of plastic scintillator detectors divided into 28 identical trapezoidal sectors each 1600 mm in length. This subdivision results in a probability for two particles from a four-nucleon phase space distributed final state hitting the same sector of less than 7%.

Each sector includes a 4.5 mm thick ΔE counter (CD), a 200 mm thick inner E counter (CI) and a 150 mm thick outer E counter (CO). The inner radius of the CD counters is 300 mm and the outer radius of the CO counters is 680 mm. Signals from the ΔE counters are used in the

event trigger logic and in particle identification, as well as in the measurement of the energy of low energy particles that stop in these detectors. Signals from the E counters are used primarily for energy measurements and in the trigger logic for neutron detection. The combined 355 mm thickness of the cylinder counters can stop protons of energy up to 200 MeV at normal incidence. The radial subdivision of the E counters into CI and CO arrays permits matching approximately 50% of the area of the ends of these counters to the photocathodes of Hamamatsu R1250 5 in. photomultipliers via UV-transmitting lucite light guides. In the CO array, the light guides are 300 mm trapezoids of the same cross section as the scintillator, coupled to 80 mm long cylinders that match the diameter of the photocathodes thus allowing for easy magnetic shielding. In the CI array, the light guides of the even-numbered counters are like those of the CO array, but for the odd-numbered counters the 80 mm cylinders are replaced by cylinders 450 mm in length whose sides are cut out to clear the photomultipliers of the neighboring counters. Thus, in the inner array, the phototubes of the odd-numbered counters are arranged behind those of the even-numbered counters. The length of the guides virtually eliminates any geometrical effects on the amount of light reaching the photocathode due to the transverse position of the incident particle. A 30 mm gap between the CI and CO counters provides for the future possibility of adding photon converters to enhance the efficiency of neutral pion detection.

After some experimentation, a wrapping method that maximizes the collection of light was developed. Each E counter is wrapped in two layers of 25 μm thick aluminum foil. A single layer of 25 μm thick aluminized Mylar between the counters prevents cold welding of the aluminum due to the pressure exerted by closely packed neighboring counters. Strips from the Mylar foil wrapping of the inner array extend around the ΔE counter to provide mechanical support for these long, thin scintillators.

The 28 trapezoidal scintillators that make up the CI and CO layers of the cylinder are packed tightly together and

bound with steel bands around the light guides at either end to form a rigid, self-supporting structure. The light guides are slightly larger than the corresponding counters so that the mechanical stress is born entirely by the light guides and the Al wrapping of the scintillators is not forced into optical contact with the surfaces.

The detector material is Bicron BC-408 plastic scintillator, which has several advantages over inorganic scintillators for the detection of pion absorption events: it is relatively inexpensive; the neutron detection efficiency for the thicknesses used in the detector is about 40%; the short decay time of the light, 2.4 ns, permits good timing resolution and operation at high rates; and the long bulk attenuation length, 3800 mm, improves light collection. These qualities outweighed the relatively low sensitivity to photons and therefore to neutral pion backgrounds, due to the long radiation length of 43.7 g/cm^2.

Prior to construction, a prototype E detector was tested with pion and proton beams. An energy resolution of 2.2% FWHM for 100 MeV protons was observed, and the time-difference distribution of signals from the two ends had a FWHM resolution of about 500 ps, equivalent to about 30 mm spatial resolution in track position along the detector.

A photomultiplier base design was developed that achieved linearity over the required dynamic range of 400. The essential trick to the design is to derive the linear signal from the 10th stage of the 14-stage tube, and to amplify these signals as needed elsewhere in the electronics to allow the tube to operate at low average current even in a high rate environment.

All plastic detectors are equipped with LEDs, with each cylinder scintillator having an LED at each end and the endcap each having two LEDs. The first function of the LED system is to monitor the gain stability of each detector. The second function is to stabilize the count rate by pulsing each LED with a constant rate of 1000 Hz, thus reducing gain variation arising from the changing beam intensity.

2.2. ΔE Counters

The design of the ΔE counters was governed by a compromise between mechanical constraints and the requirements upon energy and timing resolution necessary to provide particle identification. They are also made of BC-408 and are 1600 mm in length. They have a trapezoidal cross section 4.5 mm in thickness with an inner side 66.3 mm in width. The light guides are made of UV-transmitting lucite with an adiabatic-twisted-strip design, which was found to collect and transmit 20% more light than fish tail designs and 100% more light than optical fiber light guides. The scintillators were coupled to 1 in. Hamamatsu R1355 phototubes.

A minimum ionizing particle striking a ΔE counter at its center produces approximately 25 photo-electrons in the phototube at each end. In the analysis of the data these signals are combined to improve the resolution of the measurement. The geometric mean of the signals yields the most
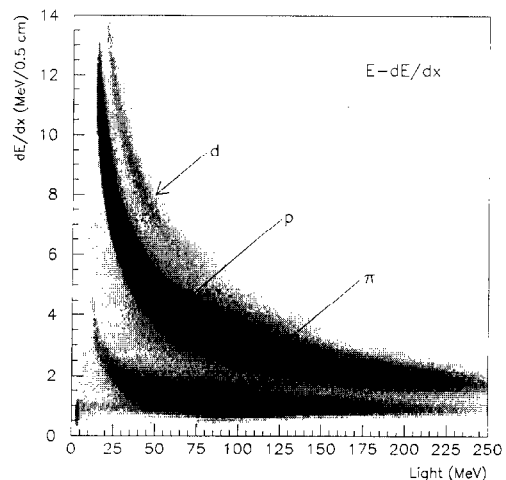

Fig. 2. The plastic scintillator E- dE/dx PID plot following the interaction of 239 MeV π^+'s with N. The different particle types are clearly separated.

nearly position-independent measurement of the energy, and the arithmetic mean of the arrival times of the light at the phototubes yields the best measurement of the the particle's time-of-flight (TOF). The efficiency of particle identification for penetrating particles is visible from the ΔE–E plots in Fig. 2. It is also possible to identify particles using E-TOF, in which the TOF is calculated from the timing information, normalized to the length of the flight path determined by the wire chambers. This method, illustrated in Fig. 3, is the only one possible for slow particles that do not penetrate into the E-counters.
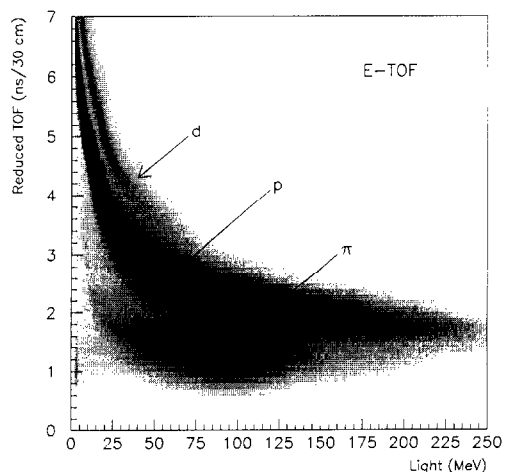

Fig. 3. The plastic scintillator E-TOF PID plot following the interaction of 239 MeV π^+'s with N. Clear bands are visible for pions, protons, and deuterons.

2.3. End-cap scintillators

End-cap detectors, made of plastic scintillators, close the ends of the cylinder except for openings to permit passage of the beam and to make room for the wire chamber mechanics and devices for target positioning. With the end-caps the counter array covers 98.8% of 4π steradians. However, only one of the wire chambers covers the end-cap acceptance, so the reconstruction of a trajectory for charged particles in this region is limited to cases in which the event vertex has been determined from other particles. Therefore, at least one charged particle must pass through both chambers for trajectory information to be available, effectively limiting the actual geometrical acceptance in a manner dependent on the distribution of particles.

Each end-cap forms an annulus with an inner radius of 88 mm and outer radius of 258 mm that fits snugly inside the ends of the outer wire chambers. The end-caps are divided azimuthally into 14 sectors, each including a ΔE counter (ED) and two E counters, arranged in concentric rings. The ED are 5 mm thick wedges of plastic scintillator that cover the front of the E counters. To match the generally higher energies possessed by forward-going particles, the downstream E counters are 400 mm long, whereas the upstream counters are 300 mm long, leaving 900 mm between the faces. The backs of the E counters are coupled to photo-tubes by lucite light guides that, in a fashion similar to that of the cylinder array, are trapezoidal for a length of 150 mm and cylindrical for a further 80 mm. Philips XP2312B 3-in. photomultipliers are attached to the outer E counters (EO), and Philips XP2262B 2-in. phototubes to the inner counters (EI). The areal matching between the scintillators and the photocathodes is about 50%.

The 14 element ED array is shifted in azimuth by half a sector with respect to the E sectors, so that the combined information from ΔE and E counters can be used to improve the angular resolution.

A wrapping scheme similar to that of the main cylinder was used (to provide the most efficient and uniform light collection in the end-cap counters as well). The counters are tightly packed around a co-axial steel tube to which they are secured with two layers of strapping tape. This tube is in turn cantilevered on a carriage that can be moved with relative ease to remove the end-cap as a unit.

In the design of the ΔE detectors, the main difficulty centered on conducting the scintillation light to the photomultipliers. The only possibility allowed by space constraints was to couple the scintillators through a 90° bend to a 5 mm thick light guide running between the outer end-cap detectors and the main cylinder detectors. This flat light guide is matched to a 1-in. Hamamatsu R1355 photomultiplier with a fish-tailed light guide. A Monte Carlo simulation showed that the best geometry for the 90° bend is a mirrored 45° bevel at the corner. To reduce the position dependence of the response of the wedge-shaped ΔE counters, the edge closest to the beam was painted black. The light guide unavoidably presents a 5 mm layer of inert material between the end-cap and the main cylinder.

2.4. Multi-wire proportional chambers

Two cylindrical multi-wire proportional chambers are included in the LADS detector to determine particle trajectories and the location of event vertices. Each chamber measures both the azimuthal angle, ϕ, and position along the beam axis, z. They are designed to provide good multiple hit resolution and to cover as much solid angle as possible, while minimizing the material in the paths of the particles.

The outer chamber (OCH) is positioned just inside the main cylinder ΔE counters. It has an anode diameter of 560 mm and an active length of 1600 mm. The inner chamber covers the region between the end-caps and has an anode diameter of 128 mm and an active length of 900 mm. After the first LADS run the original single plane inner chamber (SICH) was replaced by a concentric double plane inner chamber (DICH). The second inner chamber plane operates in a logical "or" with the first, increasing the efficiency with which particles are detected, and rendering the determination of the absolute efficiency of both planes more accurate. Lastly, each inner plane has a small dead zone near its middle; by offsetting these regions, their effects are mainly eliminated.

The mechanical structure for each chamber consisted of two Rohacell [3] cylinders which formed the substrate for the cathode planes (the DICH had three, one of which was shared between the two sub-chambers). The anode wires were strung in the gap between these cylinders. The anode wires are gold plated, 20 μm diameter tungsten–rhenium wires stretched with a force of 0.6 N. A 4 mm wide Rohacell ring at the center of the OCH, occupying the cathode to anode gap, provides additional support for the wires. Similar support rings have been added to the DICH after encountering wire stability problems attributed to shrinking of the chamber. The placement accuracy of the wires is better than 50 μm.

The cathode foils of all chambers consist of a 700 Å layer of aluminum evaporated onto a 50 μm Kapton foil. In the original chambers, accurately placed conducting strips were produced by mounting the foils in a computer controlled drafting machine and removing a succession of 0.6 mm wide lanes of aluminum with an air driven dentist's drill mounted in the pen holder assembly. The strips for the new DICH chamber were etched with a thin thread soaked in a strong base. Inner and outer cathode foils are supported by the Rohacell drums that give the chambers their shape. The anode to cathode gaps are 4 mm in the outer chamber and 3 mm in the inner chamber. The external surfaces of the chambers are covered with aluminized Kapton ground foils glued to the Rohacell. Chamber parameters are summarized in Table 2.

In the outer chamber, the angle of the cathode strips with respect to the beam axis is about 45° in order to provide the best position resolution. In the inner chambers this an-

Table 2
Relevant MWPC parameters

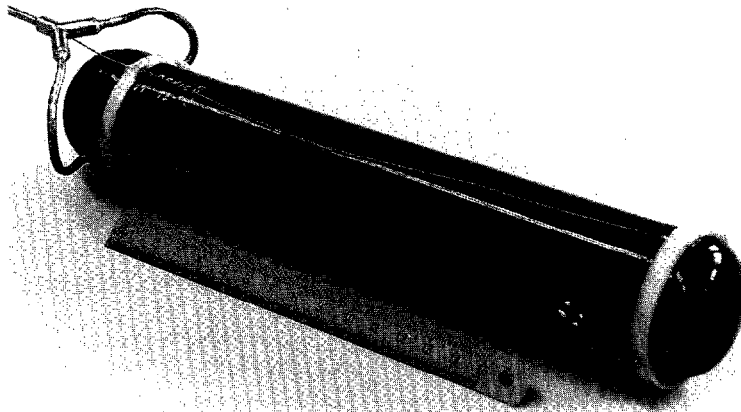| MWPC Specifications	SICH	DICH	Outer
Radius [mm]	64	112/128	280
Number of anode wires	192	144/176	832
Anode wire spacing [mm]	2.094	2.444/2.285	2.114
Number of cathode strips	384	384/384	560
Cathode strip width [mm]	2.7	3.2,2.5/3.2,2.4	3.8
Cathode strip spacing [mm]	0.6	0.6	0.6
Strip angles (inner, outer plane) [°]	34.3,41.2	14.5,24.6/24.0,19.7	45.9,44.2
Anode–cathode gap [mm]	3	3/3	4
Anode HV [V]	+2350	+2200/+2300	+2800

Fig. 4. A photograph of the LADS gas target.

gle is reduced and the strips are split in the center so that a given strip does not cross a strip of the outer cathode plane more than twice, reducing ambiguity in the reconstruction of tracks. In the DICH design, the strip angles are further reduced, sacrificing position resolution in favor of better multiple hit resolution. The loss in resolution is largely compensated for when position information from both chambers is combined.

The chambers are continuously flushed at a rate of 20–30 ml/min with a premixed room-temperature mixture of 49.8% C_2H_6, 0.2% Freon, and 50% Ar. The flow rate through each chamber is monitored with bubblers at the exhaust; safety bubblers at the intake prevent over pressure. The chambers were operated with positive HV, which was logged approximately every second by the data acquisition computer. The chamber currents were less than 1 μA in the absence of beam but increase to between 5 and 20 μA in the inner chambers when beam is present, depending on its intensity.

2.5. High pressure gas target

A major part of the LADS experimental program involves observation of absorption reactions in He isotopes. The multi-nucleon final states often contain low energy protons that would not escape from a liquid target of practical construction. Therefore, a high pressure (100 bar) gas target was constructed, modern material technology providing a sufficiently thin-walled container.

The target cell was made by Dornier Ltd. [4] of a carbon fiber compound material. Three layers of carbon fiber were alternately wound around an aluminum core in the longitudinal and azimuthal directions, glued together with epoxy resin. After etching off the aluminum, a 10 μm Cu and a 20 μm Ag layer were electroplated on to make the container gas tight. The final target wall thickness was 520 μm.

The geometrical design of the target was driven by the desire to maximize simultaneously the target thickness while minimizing the background and the energy loss of final state nucleons. The target has an overall length of 257 mm and an inner diameter of 40 mm, with rounded end-caps (see

Fig. 4). At the transitions between the target cylinder and end-caps, the wall is reinforced to a thickness of 1.2 mm at one end and 1.2 mm at the other. At the thicker end, two 3 mm stainless steel filling tubes are mounted on opposite sides. These are joined into a single tube that leads to the gas handling system. The fill tube is supported from above by a small sled that runs in a track, used for longitudinal positioning. Accurate transverse positioning is accomplished with three 0.5 mm diameter wires which run the length of the detector and which pass through two plastic rings attached at the ends of the target.

The target requires careful handling due to the brittleness of the carbon fiber (which can tolerate neither bending nor shock). Gas exchange is performed in situ to minimize the effort and risk involved in repositioning the target. For most gases the target can be filled with a simple gas handling system. However, bottles of high pressure ^{3}He gas are not available, and it is also necessary to recapture the expensive ^{3}He from the target. A cryogenic compressor built at PSI was used to pressurize the target and to recover the ^{3}He. The compressor works by cryoadsorption. A container filled with coconut charcoal is cooled in liquid ^{4}He and then adsorbs ^{3}He at small underpressure. Upon warming, pressures of up to several hundred bar may be realized [5]. For safety and to avoid lengthy filling procedures in the experimental area, the cryo-compressor is used to fill storage tanks instead of filling the target directly.

The target has been operated at pressures ranging from 13 to 100 bar with a variety of gasses: ^{2}H, ^{3}He, ^{4}He, N, Ar, and Xe. There was only one target failure. This was a slow leak which led to a gradual loss of pressure.

2.6. Pion beam

A system of slits, counters, and associated electronics logic selects from the flux of incident particles a pencil beam of pions confined to the vicinity of the target axis with minimum intensity at the target walls and in which only a single pion is present in the apparatus during the duration of an event. The logical signal BEAM, derived from these counters, is counted for the calculation of cross sections and also defines the overall event timing in the electronics.

The counter system is made up of two counters in the beam and a 64-element scintillator hodoscope (HODO) at the intermediate dispersed focus of the beam line which measures the beam momentum. A single or adjacent double hit in this hodoscope is required in the beam logic. A timing scintillator, S_{time}, on the beam axis 1980 mm upstream of the center of the target, covers most of the pion beam. Two of these have been used: in the first LADS run S_{time} was 100 mm in diameter and 3 mm thick, and in the second run S_{time} was 40×70 mm and 1 mm thick. Two discriminator levels are set on the output from S_{time}: S_{time}^{low}, below the pulse height corresponding to a single pion; and S_{time}^{high}, above the single pion pulse height but below that of two pions or a proton. Beam bursts containing a single pion are selected by the

logic $S_{time}^{low} \oplus \overline{S_{time}^{high}}$. To reduce the possibility of contamination a further constraint on the beam was imposed, requiring that no other particle be present in the three beam bursts (60 ns) that precede or follow an event.

Measurement of the time of flight over the 22 m length of the beam channel is part of the particle identification logic. The time reference for the time of flight measurement is the RF-signal derived from the accelerator, which is synchronized with the arrival of protons on the production target. The coincidence window was 5 ns for the logic:

$$RF \oplus S_{time}^{low} \oplus \overline{S_{time}^{high}} \oplus HODO.$$

A pencil beam is formed by requiring that particles pass through a 1 mm thick beam defining scintillator, S_{beam}, 390 mm upstream of the target. The 20 mm diameter of S_{beam} was smaller than the 40 mm diameter target cell in order to minimize background from the walls. Typically, 10^6 pions were incident on S_{time} each second, resulting in a BEAM rate of 10^5/s.

Particles that do not pass through S_{time} are blocked by a 200 mm thick wall of lead and a scintillator veto shield on the upstream side of LADS.

3. Data acquisition

3.1. Electronics and trigger

The trigger system has two demanding functions: to present signals to the analog to digital converters (ADCs) and time digitizers (TDCs) with good resolution and stability; and to provide an effective and flexible trigger. In addition, it must be able to handle a dynamic range of 400 for the amplitudes of the analog signals in order to provide for the detection of a neutron depositing as little as 2.5 MeV at the far end of a scintillator, and a proton depositing several hundred MeV at the near end.

Signals from each photomultiplier drive specially designed Fast Discriminator Mean-Timer modules (FDMT 300s) that contain both logical and analog sections. At the input to the FDMT the signal is conditioned by a feed-back circuit that filters out low frequency noise (<1 kHz). This allows the thresholds of the constant fraction discriminators in the logical section to be set at 15 mV with ± 3 mV channel to channel variation. The outputs from these discriminators go to the trigger electronics and, after a 300 ns logic delay, to TDCs and pattern units. The signal widths are set to 70 ns. In the analog section the signals are attenuated by a factor 0.3 or 0.4, to match the ADC range. It is necessary to AC-couple the signals at the ADC input to remove ground loop noise picked up in the 300 ns long delay cables.

The trigger decision is based on the apparent population of charged and neutral particles in an event. The trigger outputs from the FDMTs drive logic circuits (PLB300s) that contain Programmable Array Logic chips. The PLB300s

determine which sectors were hit and whether the particle was charged or neutral. The charged or neutral decision is based on whether the ΔE counter detected the particle. In the cylinder, the decision is simple: for a sector i, a charged particle is signaled by $C(i) = \Delta E(i)$, and a neutral by $N(i) = \overline{\Delta E(i)} \oplus (CI(i) \cdot CO(i))$. The signals from only one of the two photomultipliers on the cylinder counters are used in the trigger.

In the end-caps, the logic is more complicated because of the half-sector displacement of the ΔEs with respect to the E counters:

$$C(j) = \Delta E(j),$$

$$N(j) =$$
$$\left[\overline{(\Delta E(j) \cdot \Delta E(j+1))} \cdot (EI(j+1) \cdot EO(j+1)) \right]$$
$$\oplus (EI(j) \cdot EO(j)),$$

where the ΔE counters j and $j + 1$ each partially cover the E-counter j. Note that this logic registers an event with a charged particle in $\Delta E(j)$ and $E(j)$ and with a second charged particle in $\Delta E(j+1)$ and $E(j+1)$ as 2C1N (two charged particles and one neutral particle) rather than as 2C0N (two charged particles only).

The PLB300 outputs, which are organized by sector, go to a second logic circuit, PLB301, that uses look-up memory (EPROM) to count the total number of charged and neutral particles in each event. For example, outputs signalling the arrival of 0C (no charged particles), 1C, 2C, $\geq$1C, $\geq$2C and $\geq$3C particles are provided. Signals indicating similar multiplicities of neutral particles are also provided, as well as independent outputs signaling $\geq$1C or $\geq$2C in the cylinder or in the end-caps.

Coincidence with an incident pion is established by strobing the PLB300s and PLB301s with the logical signal BEAM. The PLB301 outputs are combined using standard NIM electronics to form the exclusive multiplicities: 0C1N, 0C$\geq$2N, 1C0N, 1C1N, 1C$\geq$2N, 2C0N, 2C$\geq$1N, and $\geq$3C. These signals are then passed through adjustable prescalers to the master trigger. Interesting events, for example $\geq$3C, have little or no prescaling while others, for example 1C0N, have large prescale factors adjusted so that these events comprise about 10% of all triggers. In addition to these physics triggers, other triggers were generated for signals from the LED monitoring system, a random sample of the beam, and for a clock synchronized to the cyclotron RF. The OR of all these forms the trigger for the event read-out.

The outputs from each stage of the trigger (FDMT, PLB300, PLB301, NIM logic, prescaler) are recorded in latches, and all but the first two in scalers as well. Comparison of latches set by the various stages of the trigger decision is used to study the internal consistency of the logic. The physics triggers do not perfectly select the multiplicities, although logic errors in the electronics are not the main reason. Possible sources of error are:

a) punch-throughs from the end-cap to the barrel;
b) signals in adjacent sectors induced by one particle, either due to the geometry of the event or to the particle reacting in the plastic;
c) two particles in the same sector;
d) random hits;
e) electronics errors.

The last two are correlated since the main source of errors from the electronics is due to nearly out-of-coincidence pulses.

Errors in the trigger type should not cause errors in the data analysis, so long as it is correctly recorded which trigger (output from the mCnN NIM coincidence) generated the event being analyzed. However, such errors lead to imprecision in selecting the multiplicities, and require that all physics triggers be analyzed to find all of a particular event type of interest. A serious error, such as misidentifying interesting events in the trigger as ones with very high prescale factors, for example mistaking 2C$\geq$1N as 1C$\geq$1N, would result in most of these events being thrown away, even though the overall normalization of those kept would be correct. Further, some classes of potentially interesting events, such as 1C1N, are substantially rejected in this scheme due to the very large background from hits in adjacent sectors caused by a single particle, which are recorded as 1C1N by the logic.

3.2. Data processing

The LADS data acquisition system is built of Fastbus, CAMAC and VME modules connected to a cluster of three Vaxstation 4000/90s through a Turbochannel-VME interface (Fig. 5).

The cathode strips of the multi-wire proportional chambers drive LeCroy TRA1000 current sensitive preamplifiers mounted close to the chambers. These in turn drive amplifiers through 50 m of twisted pair delay cable. These 1328 signals along with the 280 analog signals from the photomultipliers are presented to eighteen 96-channel Fastbus ADCs (LeCroy 1885), which have a resolution of 12 bits, a range of about 1350 pC, and a conversion time of 275 μs. The ADCs are read via FASTBUS by a Segment Manager Interface (SM/I LeCroy 1821), that can read ADC data at >25 MB/s, perform hardware pedestal subtraction, and suppress empty channels. Typically this step reduces the volume of data by 96%. The compressed data are stored in the memory of the SM/I module and are read at a rate of 1.3 MB/s during the event building stage by an AEB Fastbus processor (Struck STR-501) using an interface designed at CERN [6].

The 280 logic signals from the photomultipliers are passed to eleven 32-channel FASTBUS TDCs (Phillips Scientific 10C6). These convert the signals and suppress empty channels within 8 μs. The logic signals are also fed to three 128-channel FASTBUS latches (Phillips Scientific 10C8). Two more latches are used to register the trigger patterns
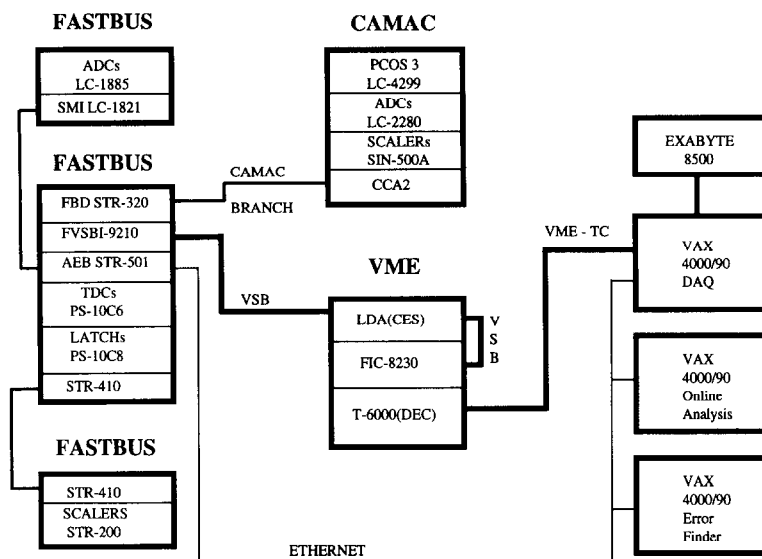
Fig. 5. A simplified picture of the LADS data acquisition system.

presented by the PLB 300, PLB 301 and the beam particle hodoscope. All TDC and latch modules are read by the AEB processor using the block-readout mode in which the 100 μs overhead for starting a fastbus block transfer occurs only once for all 16 modules.

Each of the 1280 anode wires in the multi-wire proportional chambers drives a current sensitive, differential input amplifier-discriminator housed on LeCroy 2735 cards containing 16 channels, each located as close as possible to the chambers. These produce logical signals that are stored awaiting a trigger and then processed by the PCOS III System (LeCroy 2731, 2738). The clusterized information characterizing the pattern of wire hits is passed to a CAMAC buffer (LeCroy 4299) that is read by the AEB processor through a FASTBUS–CAMAC interface (FBD, Struck STR-320). This interface also reads a set of 6 CAMAC scalers (SIN-500A) and two CAMAC ADCs (LC 2280) that encode control and diagnostic signals. All CAMAC readout is done through FASTBUS block transfer cycles that are translated by the FBD module into standard CAMAC block cycles. Additional signals are counted by three 32-channel, 32-bit FASTBUS scalers (Struck STR-200).

Event building is done by the AEB processor running the OS-9 operating system. Most of the software is written in Real-Time Fortran [7]. In order to reduce the overhead for FASTBUS data block-reads the standard FASTBUS library routine (FBRD) was replaced by a simpler assembler routine that reduced the overhead from 200 to 100 μs. The dead-time for reading an event is about 1 ms, including digital conversion, readout, and event building. The average event size is 150 words (600 bytes), and events are buffered by the AEB into 32 kbyte data blocks.

Scalers are read once per second and at the beginning and end of each run. Full data buffers are written by the AEB

to a dual-ported memory in the FASTBUS-VSB interface (CES FVSBI-9210) from which the data are read through the VSB bus by a FIC VME processor (CES 8230) and placed in the FIC's data memory. The VME is connected to one of the Vaxstation 4000/90s using a Turbochannel to VME interface (DEC MVIB/3VIA) that can perform programmed transfers (PIO) initiated by the Vaxstation or DMA transfers initiated by the VME. Since at present no device driver is available from DEC, access from the VME was not possible, thus the Vaxstation CPU does the PIO data transfers from the FIC's memory at the rather slow rate of 600 kbytes/s.

In the Vaxstation the main data acquisition process writes the data to a high density 8500 Exabyte drive (two drives in parallel can be used if needed). The other two Vaxstations are used for data monitoring and analysis. PAW is used for data display.

The performance of the acquisition system is governed by the dead-time per event and by the present speed of the Turbochannel VME interface, with both being well matched to 1000 events/s and 600 kbytes/s. Typical operating rates actually used in the final setup were 600 events/s.

4. Data analysis

4.1. Particle reconstruction

On the data tape, the information about an event is indexed by the individual counters in the detector. The first step of the data analysis is to reorganize the data into "particles". Initially, the different counters in the same sector are grouped together. The particle in that sector is considered to be charged if the ΔE fired, and neutral otherwise. In the

end-caps, each E-block is partially covered by two ΔEs; the particle is labelled charged if either has light. Next, neutrals are combined with charged particles in adjacent sectors into single charged particles. This is done since the probability of a charged particle scattering into an adjacent sector due to multiple scattering or a nuclear reaction is significantly higher than the chance that a charged particle and a neutral particle are adjacent.

More complicated cases are then examined. One example consists of those particles which have sufficient energy and the correct trajectory to pass through a corner of an end-cap and into the cylinder scintillators. These particles are reconstructed, with the end-cap information determining whether they are charged or neutral. This situation and the above mentioned adjacent neutrals account for the majority of the cases in which the hardware trigger incorrectly classifies the event, since a single particle appears to be two.

At this point the plastic information has been sorted into particles. As further information about the event is determined, such as trajectories, energies, particle identification, etc., it is stored in arrays indexed by particle.

4.2. Trajectory reconstruction

Information from the two multi-wire proportional chambers is used to calculate trajectory information for charged particles. The procedure for decoding this information is complicated by the presence of multiple particles in the final state and the fact that some pairs of the helically wound cathode strips cross twice. The first step is the determination of peak positions on each cathode plane. Then the peaks on the two planes in each chamber are resolved into hit locations, which are finally associated with particles in the plastic to determine trajectories.

A vertex can now be calculated for the event. Whenever possible, a vertex is found by using two tracks (the mean minimum separation between tracks is 1.7 mm). Otherwise, a vertex is found by taking the point of closest approach of one track to the beam line. Angles θ and ϕ are calculated for each particle using two chamber hits if they exist, or one hit and the vertex if not. At a minimum, each charged particle has to have at least one hit, and one must have two hits, in order for all to have trajectory information. The angular resolution is about $1°$, but varies with the geometry of an event.

4.3. Calibration

LADS has 280 photomultipliers whose analog (ADC) and timing (TDC) signals must be calibrated. The ADC offsets were calibrated by measuring the pedestal positions. The TDC gains were calibrated by adding known lengths of delay to the pulsed LEDs attached to the scintillators. The more complex calibrations of the ADC gains and the TDC offsets had to be determined directly from the data.

The first step of the energy calibration was performed by using the reaction $^2H(\pi^+,pp)$. This reaction can be identified by the angles of the outgoing particles using the chamber information, and the energies of each proton are likewise determined. The protons are then tracked through the LADS geometry, and the amount of light deposited in each scintillator is estimated by using the Bethe–Bloch equation and correcting for saturation effects (the formula from Ref. [8] was used). Comparing this calculated quantity to the measured value, the ADC gains were determined.

The above method used the assumption that the ADC responds linearly to deposited light. Corrections can be made to account for small non-linearities introduced by the scintillator geometry and electronic effects. These non-linearities (including possible inaccuracies in the saturation formula) were corrected for by an examination of the reactions $^3He(\pi^+,ppp)$ and $^4He(\pi^+,ppd)$. Like $^2H(\pi^+,pp)$, these reactions can be identified and the full kinematics determined by using the chambers. The difference is that the reactions on ^3He and ^4He are a source of protons at a range of energies and angles, whereas the protons from ^2H have a strict energy-angle correlation and a restricted energy range. By comparing the energies calculated from the angles to the measured energies, calibration correction curves were determined as functions of both energy and θ. This procedure provides linear energy scales in the results and the typical FWHMs of summed energy spectra improves from 6 to 3% when the corrections were applied.

The TDC offsets were determined by examining the TOF of charged particles for the ΔEs and of neutrons or photons for the E-blocks. Charged particles are not suitable for the E-blocks since they are decelerated on their way to the counter and their penetration depths vary with energy. Therefore the neutron from the kinematically over-determined reaction $^4He(\pi^+,pppn)$ was the preferred particle for the TDC calibration of these counters, because the neutrons react with nearly equal probability throughout the scintillator. An alternative method for the TDC offset calibration of the E-counters is the usage of photons from single charge exchange reactions, since their velocity is fully independent of their energy. To correct the timing calibration for global drifts due mainly to temperature variations, the offsets were normalized to the position of the timing peak in the S_{beam} spectrum for each run. To ensure that measured TOFs were not dependent on the position of the pion in the timing envelope, the signal in S_{time} was used to adjust the measured impact times for each event.

4.4. Monte Carlo simulation

A Monte Carlo program to simulate the acceptance of LADS has been developed using the detector simulation package GEANT [9]. Various specifically tailored event generators are used, and the resulting particles are tracked through the LADS geometry. Information is then provided to the LADS analysis package at the level of energy de-
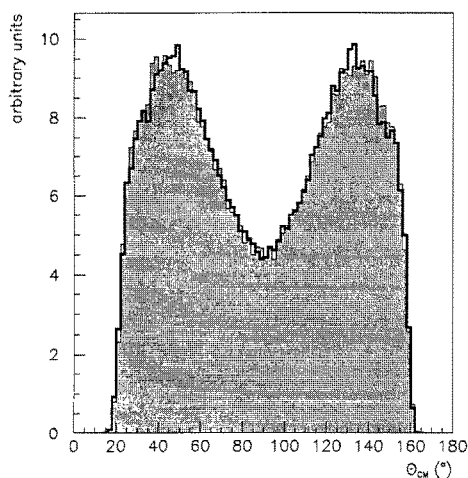
Fig. 6. A comparison of the angular distribution in the CM system of the two protons following the absorption on deuterium of 162 MeV π^+. The solid line is the data and the shaded region is the Monte Carlo simulation.
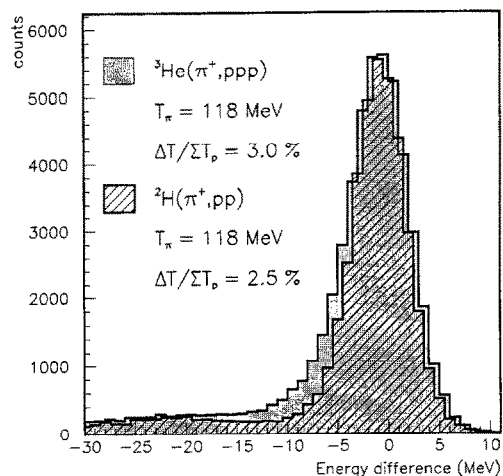

Fig. 7. The difference between the summed total energies of the initial and the final states particles measured in the ^{3}He(π^+,ppp) and ^{2}H(π^+,pp) reactions at T_π = 118 MeV.

posited in specific counters and hits on the chamber cathode strips, both smeared by the detector resolution. This information is then analyzed in the same manner as the data, and comparisons are made.

As an illustration of the capabilities of the Monte Carlo simulation, the angular distribution of the two protons following the ^{2}H(π^+,pp) reaction is presented in Fig. 6. The kinematics of the two protons were generated using the well known Ritchie [13] parametrization of the ^{2}H(π^+,pp) process. Both protons were then tracked through the LADS detector with GEANT, and the data simulating the detector response were analyzed in the same way as the experimental data. The good agreement of the experimental and the simulated data shows that the response and the acceptance of the LADS detector is well understood. In the various analyses the simulations have been used to correct the data for geometrical acceptance and energy thresholds, reactions of protons in the scintillator, the MWPC reconstruction inefficiencies, and various software inefficiencies.

5. Performance

In the previous sections, some indication has already been given of the performance of the LADS detector. In the following ones, further illustrations will be shown.

5.1. Measurement of energies

A good measure of the absolute calibration of the ADC signals is the difference between the summed total energies of the initial state and final state particles, respectively. If everything is correct, a peak should appear around 0 MeV. Fig. 7 shows such a spectrum for the reactions ^{3}He(π^+,ppp) and ^{2}H(π^+,pp) for 118 MeV incident pions. The width of

the peak is indicative of the energy resolution. It is 3% in the figure. The tails to negative energies result from reaction losses in the scintillators.

5.2. Measurement of time

There are two distinct ways in which the timing resolution is important. The first is the use of the difference between the TDC values from the photomultipliers at the two ends of the cylinder scintillators to determine the longitudinal hit position. This is of primary importance for neutral particles, and will be discussed in a following section. The second, discussed here, is the calculation of time-of-flight, used primarily for particle identification.

The information of interest is not the actual TOF, but the TOF normalized by the pathlength. Therefore the reduced TOF is defined as the amount of time it would take a particle to traverse 30 cm, which is equivalent to $1/\beta$ when measured in ns. The use of the reduced TOF in particle identification has already been shown in Fig. 3.

Fig. 8 shows the difference between the reduced TOF calculated from the detected energy of a proton and the reduced TOF measured by the TDCs. The peak appears near 0 ns as it should, and the width implies a time resolution of 750 ps after correction for the pion beam smearing. The ΔE counters in the end-cap have similar timing resolution, and in the E-counters the time resolution varies from 1.6 ns for the CO to 2.5 ns for the EI.

5.3. Measurement of angles

The angular definition of a track is governed by the spatial resolution of the wire chambers and the distance between them. In the ^{2}H(π^+,pp) reaction, knowledge of the angles θ and ϕ of one proton gives the angles θ and ϕ for the
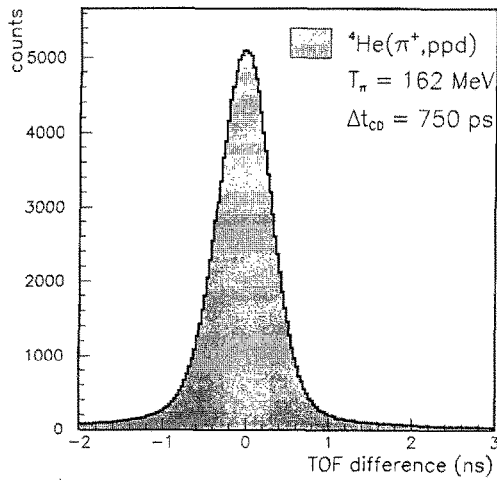
Fig. 8. The difference between the reduced time of flight calculated from the energy of a proton and that measured by the TDCs for the ^{4}He(π^+,ppd) reaction at T_π = 162 MeV.

second proton. The distribution of the differences between the calculated and measured values for these angles is shown in Fig. 9. The folded angular resolutions (FWHM) for both protons are $\Delta\theta_{pp} \approx 1.1°$ and $\Delta\phi_{pp} \approx 1.5°$. Assuming that both protons have the same angular smearing, the single particle angular resolutions (FWHM) are $\Delta\theta \approx 0.8°$ and $\Delta\phi \approx 1.1°$.
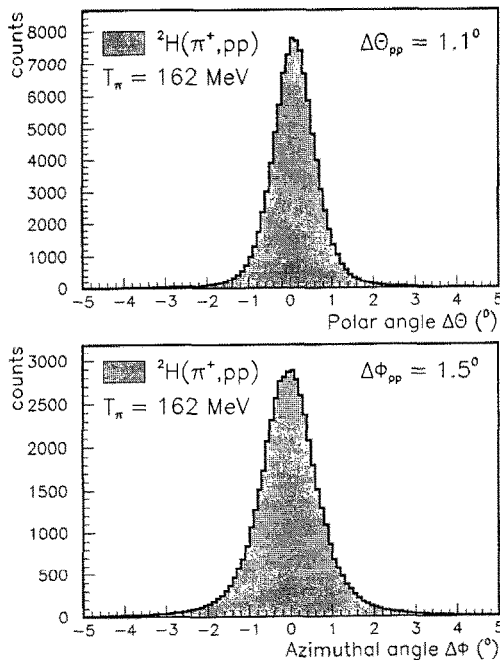

Fig. 9. The differences between the calculated and measured polar and azimuthal angles for protons from the ^{2}H(π^+,pp) reaction at T_π = 162 MeV.

Table 3
The average single particle MWPC efficiencies for absorption protons in LADS. For the DICH+OCH setup, the information from the two inner chambers was ORed

Setup	Inner chamber	Outer chamber
SICH+OCH	98	97
DICH+OCH	98	96

5.4. Efficiency of the wire chambers

Several factors determine the efficiency for the reconstruction of an event in the wire chambers. The first is the hardware-driven probability that a chamber will record a hit if a particle passes through it. Others are due to software complexities that arise when several particles pass through the same chamber; an example being events in which cathode peaks corresponding to different particles are incorrectly assigned to each other. In addition, in order to deduce trajectories for all of the charged particles in an event, it is necessary for at least one of them to produce two hits so that a vertex may be calculated, and for all of them to produce at least one hit. Since these factors depend in a complex manner on the event geometry, the MWPC efficiencies were taken into account in the simulation of the detector. First, the hardware efficiency was measured for a single particle passing through each chamber (see Table 3). These numbers were supplied to the Monte Carlo, which reproduced the patterns on the cathode strips, and then recalculated the hit positions.

5.5. Neutron detection

The two cubic meters of plastic scintillator that make up the LADS detector make it a potentially efficient neutron detector. The efficiency for the detection of a neutron depends on its energy, on the amount of scintillator it traverses, and on the light detection threshold.

The neutron detection efficiency can be determined directly from the data by using the reaction ^{4}He(π^+,pppn). By measuring the proton momenta, the neutron momentum can be determined. Calculating the efficiency is then simply a matter of measuring the fraction of the events where this neutron is actually seen. Fig. 10 shows the angle integrated neutron detection efficiency as a function of energy for neutrons following the absorption of 239 MeV π^+. The data were corrected for events in which the neutron has small momentum relative to one of the three detected protons and may not therefore have been identified as a separate particle. The figure shows good agreement between the data and the efficiency calculation used in the simulations. The efficiency approaches 40% (for a 4 MeV threshold).

The angular precision for neutron detection in the azimuthal direction is given by the sector structure of LADS (FWHM = 12.8°). The polar angle is determined from the z-position of the interaction point in the scintillator as mea-
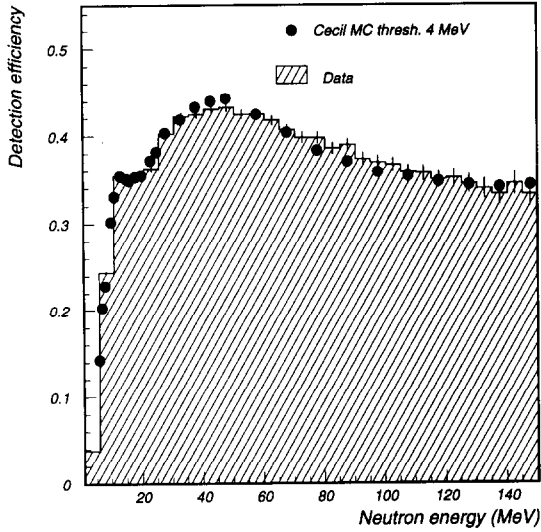
Fig. 10. The comparison of the measured LADS neutron detection efficiency (shaded area) with the Cecil [12] code Monte Carlo simulation (black dots). The data is for neutrons from the ^{4}He(π^+,pppn) reaction at $T_\pi = 239$ MeV.

Fig. 11. The neutron–gamma discrimination based on the reduced time-of-flight.

sured by the time difference of the signals at the ends of the bars. The resolution in z for neutrons detected in the cylinder will be similar to the resolution for charged protons calculated in the same manner. This resolution is determined by comparing values calculated with the chamber information to values calculated without it, and is about 75 mm FWHM.

To determine the neutron energy by measuring the time of flight, both the vertex in the target and the interaction point in the scintillator must be known. If the neutron is accompanied by charged particles, the vertex can be determined quite accurately. The z-coordinate of the interaction point can be determined by the time difference of the pulses from the ends of the bar. However, the radius of the interaction point cannot be measured; it is known only within the limits defined by the dimension of the counter. Therefore the path length of the neutron is only poorly known. Even without this problem, LADS would not be particularly well suited to the measurement of neutron energies because the typical flight path is short. The measured neutron energy resolution is about 60% FWHM.

The neutral timing resolution is, however, sufficient for the task of neutron–photon separation. An example of the LADS n-γ discrimination following pionic reactions on ^{4}He is shown in Fig. 11 for the two pion beam energies 118 MeV and 240 MeV.

5.6. Resolution of calculated quantities

The invariant mass of the unmeasured reaction products is important for the identification of the absorption reactions, frequently offering a clue to the mechanisms involved in the reaction. It is known as missing mass and is defined as:
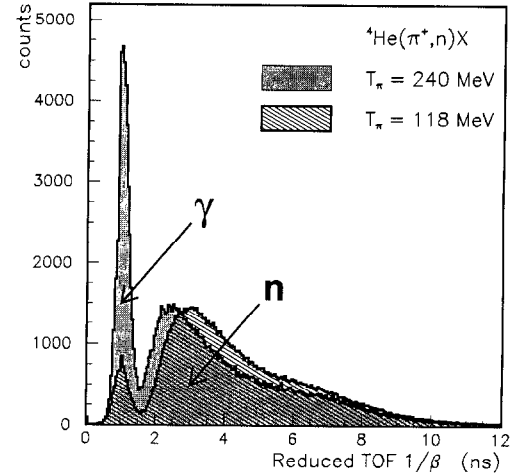
$$m_{\text{miss}} = \sqrt{\left(E_\pi + E_{\text{tgt}} - \sum_i E_i \right)^2 - p_{\text{miss}}^2},$$

with $E_\pi = T_\pi + m_\pi$, $E_{\text{tgt}} = T_{\text{tgt}} + m_{\text{tgt}}$ and $E_i = T_i + m_i$ being the total energy of the beam pion, the target nucleus, and the particle i, respectively.

$$p_{\text{miss}} = |\mathbf{p}_\pi - \sum_i \mathbf{p}_i|$$

is defined as the missing momentum of the reaction with $\mathbf{p}_\pi$ and $\mathbf{p}_i$ as the momenta of the pion and the final state particle i, respectively.

Resolution in missing mass involves both energy resolution and angular resolution. A typical missing mass spectrum of the reaction ^{3}He(π^+,pp)p is shown in Fig. 12. In this reaction only two protons are measured, but the momentum of the third can be unambiguously reconstructed. The peak appears at $m_{\text{miss}} = 939.4$ MeV/c^2, which is in good agreement with the proton mass of 938.3 MeV/c^2. The excellent resolution, $\Delta m_{\text{miss}} \approx 8$ MeV/c^2, permits efficient rejection of background from misidentified pions. To the right side of the missing mass peak we see a tail originating from reaction losses in the scintillators.

Fig. 13 shows the missing momentum spectra of the reactions ^{3}He(π^+,ppp) and ^{2}H(π^+,pp). Since all final state particles were measured, no momentum should be missed. The widths of the distribution thus reflects the resolution for recoil momentum spectra, which are commonly used in pion absorption studies to identify different absorption processes. The missing momentum resolution, $\Delta p_{\text{miss}} \leq 15$ MeV/c, is significantly better than the minimal design goal of LADS. The relevant resolutions of the LADS detector system are summarized in Table 4.

Table 4
Summary of important LADS resolutions (FWHMs)

| Reaction	Variable	Total	Single particle
^{2}H(π^+,pp)	Proton kinetic energy	$\Delta T/T = 2.5\%$	$\Delta T = 4.5$ MeV
^{3}He(π^+,ppp)		$\Delta T/T = 3.0\%$	$\Delta T = 4.3$ MeV
^{4}He(π^+,pppn)	Neutron kinetic energy	$\Delta T/T \approx 60\%$	
^{2}H(π^+,pp)	Proton polar angle	$\Delta\Theta_{pp} = 1.1°$	$\Delta\Theta_p = 0.8°$
^{2}H(π^+,pp)	Proton azimuthal angle	$\Delta\phi_{pp} = 1.5°$	$\Delta\phi_p = 1.1°$
^{4}He(π^+,pppn)	Neutron polar angle		$\Delta\Theta_n = 13°$
^{4}He(π^+,pppn)	Neutron azimuthal angle		$\Delta\phi_n = 12.8°$
^{4}He(π^+,ppd)	Time of flight		$\Delta t = 750$ ps
^{3}He(π^+,pp)p	Missing mass	$\Delta m_{miss} = 8$ MeV/c^2	
^{2}H(π^+,pp)	Missing momentum	$\Delta p_{miss} = 10$ MeV/c	
^{3}He(π^+,ppp)		$\Delta p_{miss} = 15$ MeV/c	
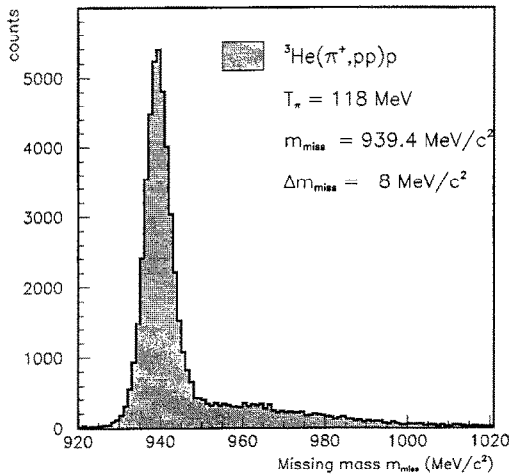
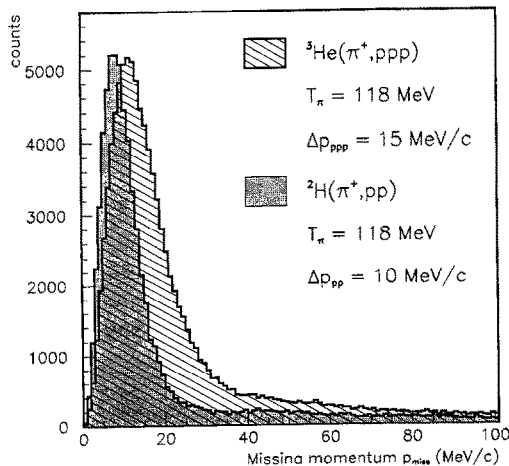Fig. 12. The missing mass reconstructed in the ^{3}He(π^+,pp)p reaction at $T_\pi = 118$ MeV.

Fig. 13. The missing momentum reconstructed in the ^{3}He(π^+,ppp) and ^{2}H(π^+,pp) reactions at $T_\pi = 118$ MeV.

6. Conclusion

A Large Acceptance Detector System has been designed and constructed for the study of pion absorption in the Δ(1232)-resonance energy region. The detector has proven well suited to its tasks [10,11] and generally meets or exceeds its design goals. The detector characteristics are well understood.

References

[1] H.J. Weyer, Phys. Rep. 195 (1990) 295.
[2] C.H.Q. Ingram, Nucl. Phys. A 533 (1993) 573c.
[3] PMMA Polymethylmethacrylat (Acrylglass); Angst-Pfister AG, Thurgauerstrasse 66, CH-8052 Zurich, Switzerland.
[4] Dornier Ltd., P.O. Box 1420, D-88039 Friedrichshafen, Germany.
[5] B. van den Brandt, Ph.D. thesis, Rijksuniversiteit Leiden, 1981.
[6] U. Mueller, Private Communication, PPE Division, CERN, CH-1211 Geneva, Switzerland.
[7] Real-Time Fortran,H. von der Schmitt, Physikalisches Institut, Universität Heidelberg, Germany.
[8] R. Madey et al., Nucl. Instr. and Meth. 151 (1978) 445.
[9] GEANT 3.21, CERN Program Library, CN Division, CERN, Geneva, Switzerland.
[10] T. Alteholz et al., Phys. Rev. Lett. 73 (1994) 1336.
[11] D. Androić et al., in preparation.
[12] R.A. Cecil, B.D. Anderson and R. Madey, Nucl. Instr. and Meth. 161 (1979) 439.
[13] B.G. Ritchie, Phys. Rev. C 44 (1991) 533.